Journal of Geointerface, Vol. 4, No. 1, July 2025, pp. 29–37 e-ISSN: 2583-6900

Modelling fault networks in the Shizidun tungsten deposit in Yangtze Block, South China Craton

Awei Mabi [1,*], Niuben Yu[2], Hao Zhong[2], Dekang Chen[2], Jizhong Tong[2], Linbing Yu[2]

[1] *Nanchang Institute of Science and Technology, Nanchang 330000, China*
[2] *The Second Geological Team of Jiangxi Geological Bureau, Jiujiang 332000, China*

ABSTRACT

This study integrates field observations, structural analysis, and drillhole data to model the complex fault networks within Shizidun tungsten deposit in the central-northern Yangtze Block of South China Craton by using ArcGIS and Leapfrog software. Surface mapping revealed small-scale faults with diverse orientations, including ENE-, NW-, and N-S-trending faults, while subsurface modelling using drillhole data identified a network of steeply dipping faults intersecting within a Neoproterozoic granitic pluton which was intruded by Mesozoic granites. The results highlight a structurally complex subsurface environment, likely influenced by regional E-W strike-slip tectonics, which controls tungsten mineralization and poses potential geohazard risks. These findings enhance our understanding of the deposit's geological framework, providing insights for targeted mineral exploration and geohazard mitigation in the region.

ARTICLE HISTORY

Received: 07 March 2025
Revised: 04 April 2025
Accepted: 12 April 2025

https://doi.org/10.5281/zenodo.15205686

KEYWORDS

South China Craton
Shizidun
Fault networks
Leapfrog 3D modelling
Geohazard Mitigation

1. Introduction

Fault systems are fundamental geological structures that exert a profound influence on both mineral exploration and geohazard management. These planar discontinuities in the Earth's crust serve as conduits for hydrothermal fluids, pathways for magma ascent, and zones of mechanical weakness that control the localization and distribution of mineral deposits. In the context of tungsten metallogeny, faults play an especially pivotal role, acting as structural traps that facilitate the precipitation of economically valuable minerals such as scheelite and wolframite. The Shizidun tungsten deposit, located in the northern Jiangxi province within the center-northern Yangtze Block, exemplifies this relationship, where fault networks have governed the emplacement and enrichment of tungsten mineralisation. Understanding the geometry, kinematics, and evolution of these fault systems is therefore essential for optimizing exploration strategies and unlocking the mineral potential of this region.

Beyond their significance in resource exploration, fault systems are equally critical in the assessment and mitigation of geohazards. Active or reactivated faults can trigger seismic events, landslides, and ground subsidence, posing risks to infrastructure, mining operations, and local communities. In tectonically complex regions like South China Craton, where multiple phases of deformation have shaped the geological framework, the interplay between fault activity and surface processes amplifies these hazards. Faults in the Shizidun deposit serve not only as a tool for delineating mineralized zones but also as a means of safeguarding against geohazard-related disruptions. By modelling the fault systems in this area, we can better predict zones of instability

*Corresponding author. Email: mabiawei@ncpu.edu.cn (AM)

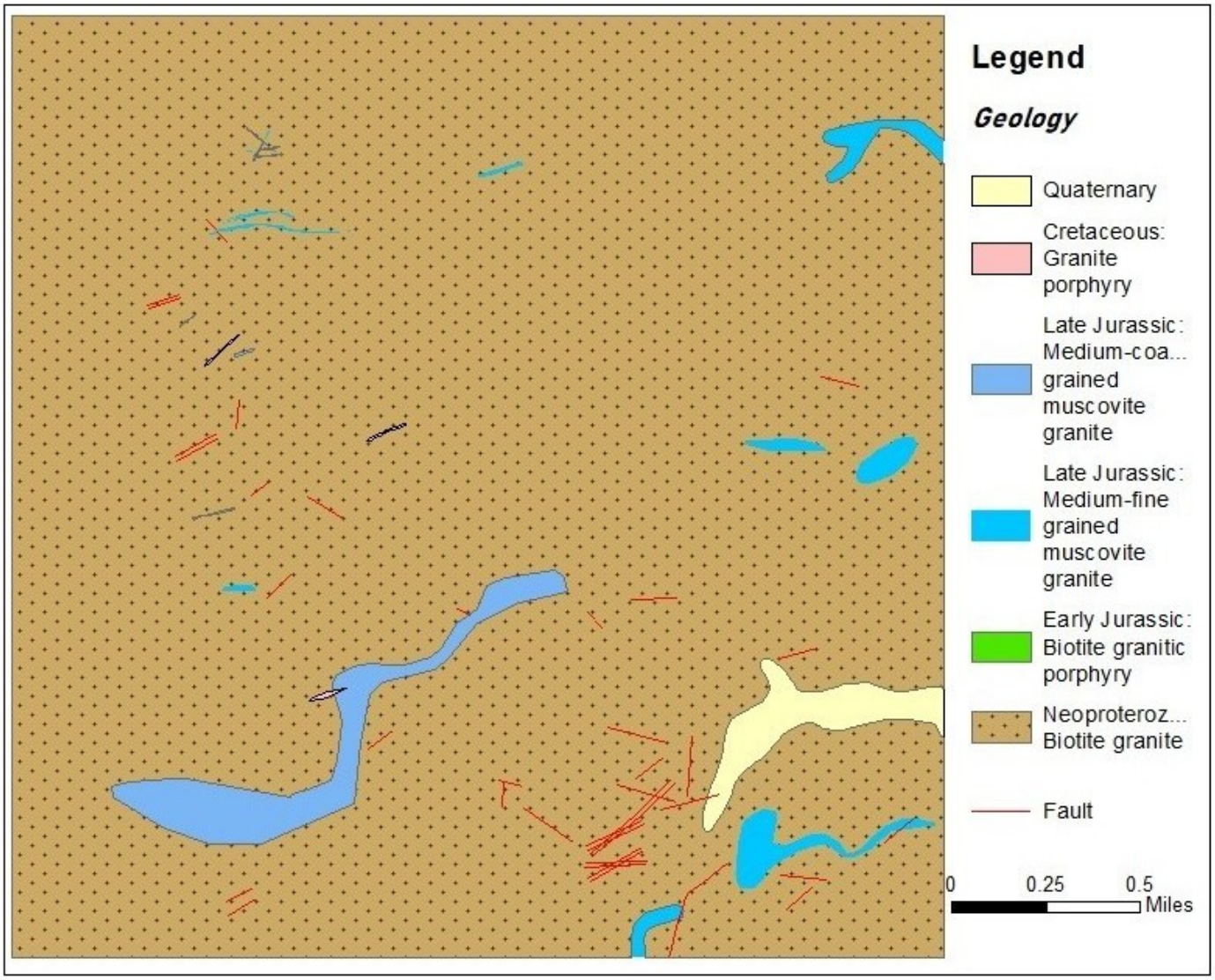

Fig. 1. Geological map of Shizidun tungsten deposit (the precise geographic coordinates cannot be disclosed on the map due to commercial sensitivities).

and implement protective measures that enhance operational safety and environmental resilience.

In the past, studying fault systems greatly relied on the field investigation and interpretation of remote sensing imagery. These data are typically collected through direct observation, mapping, and measurements at the surface (e.g., fault traces, orientations, and displacements). This provides high-resolution details but is limited to accessible outcrops, specific locations and dense vegetation cover, often missing subsurface continuity or faults obscured by overburden.

In contrast, Leapfrog relies on drillhole data, which samples the subsurface at discrete points (e.g., collar locations, lithology intervals, and structural measurements). While it interpolates between these points to model faults in 3D, the resolution depends on drillhole density and spacing. Sparse or unevenly distributed drillholes can lead to underrepresentation or oversimplification of fault geometry compared to the detailed surface observations from field studies.

This study focuses on the systems of the Shizidun tungsten deposit, integrating field observations, structural analysis, and drill hole data to construct a comprehensive model of their architecture by using software ArcGIS (ESRI, 2025) and Leapfrog (ARANZ Geo Limited, 2015). We aim to elucidate the structural controls on tungsten mineralization and provide insights into the broader geodynamic processes that have shaped the study region. Furthermore, this work seeks to bridge the gap between mineral exploration and geohazard protection.

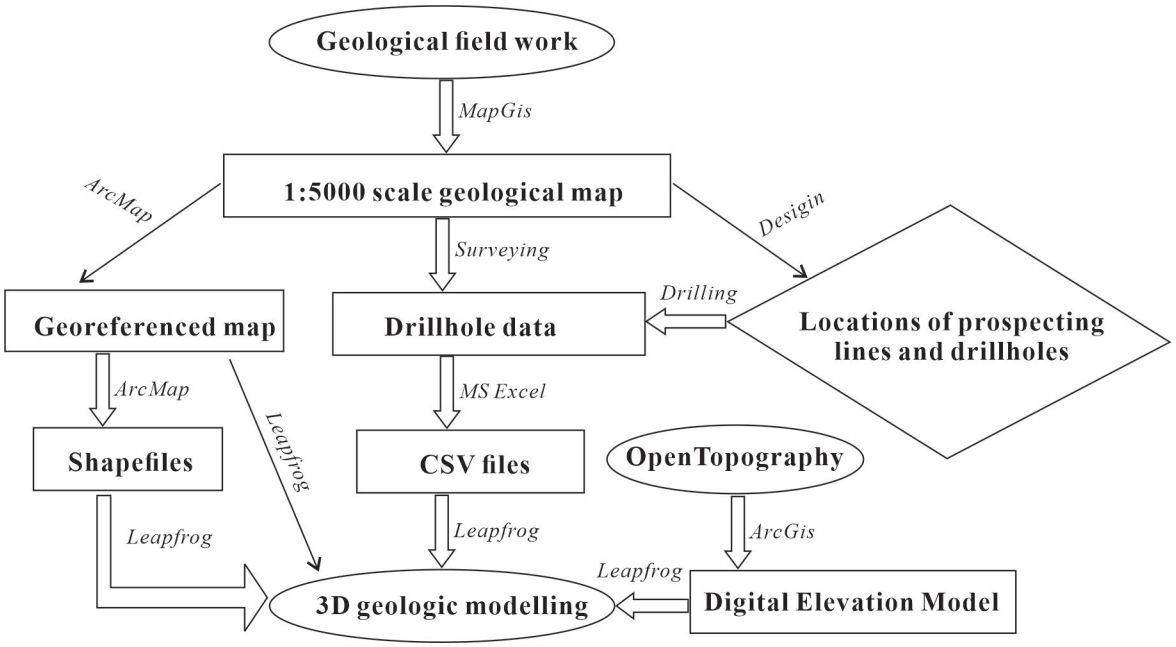

Fig. 2. The flowchart illustrating the methodology and workflow for this study.

2. Geological background

The Jiangnan porphyry-skarn W belt of the Lower Yangtze Metallogenic Province (Zhang et al., 2022) in the north and the Nanling W-Sn metallogenic belt in the south make Jiangxi Province a world-class tungsten province (Wei et al., 2018). Associated with a relatively minor amount of Cu and Mo minerals, the Shizidun W deposit is considered as the eastern extension of the supergiant Shimensi granitic-type W-Cu-Mo deposit.

The supergiant Shizidun W deposit belongs to the giant Dahutang ore field (Zhang et al., 2022) in northern Jiangxi province. Neoproterozoic and Mesozoic granites cover the studied area. In addition, the Mesozoic granites can be identified as the Early Jurassic, the Late Jurassic, and the Cretaceous granites (Fig. 1).

Faults are rarely discovered on the surface and could be grouped into the ENE-trending, the NW-trending, and the N-S-trending faults, respectively.

The largest northeast-trending fault is discovered in the southern studied area, with a length of more than 1000 m and a width of 2–20 m. The fault dips at 54° with dip direction roughly NW at the southwest part. By contrast, the northeast part shows a SE dip direction with a dip angle of 27°. Others are much smaller faults, with a length of approximately several meters and a width less than 1.7 m. The dip directions are various. They usually steep with dip angle ranging from 48–84°. A few number of faults dip at less than 30°.

The small-scale northwest-trending faults are generally ~10 m long and 0.05–0.5 m wide, dipping at 42–80° with direction roughly SW. They have a strike direction ranging from 295–304°. The tiny N-S-trending faults are rarely observed, with lengths around 10 m and widths of 2–50 cm, dipping at 60–71° with diverse directions.

3. Methodology

The drillhole data are collected from the exploration project carried out by the Second Geological Team of Jiangxi Geological Bureau, making it possible to get the Comma Separated Values (CSV) files named Collar, Survey, and Geology, respectively, for leapfrog 3D modelling. A 1:5000 scale geological map was obtained by using traditional mapping methods. The original map was produced by the Chinese standard software MapGis. We georeferenced the map in JPEG format by using ArcMap and digitalize the surface faults into shapefile format.

Drillhole data in CSV format, the georeferenced map, and the shapefiles of the digitalized faults were imported into Leapfrog, where 3D modelling was performed using implicit modelling techniques. The methodology and workflow can be represented in a flowchart (Fig. 2).

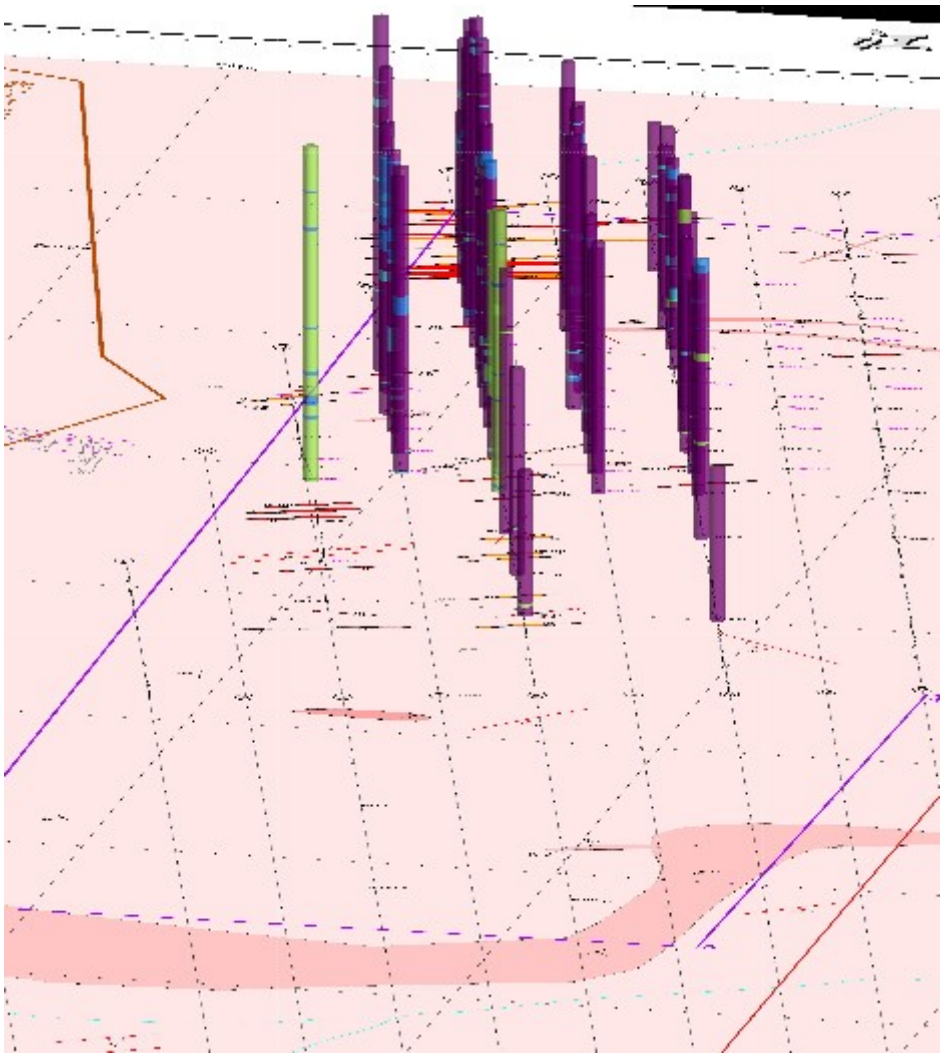

Fig. 3. Leapfrog locates the drill holes in the exact places on the georeferenced map (The data of geographic coordinates of drill holes for Leapfrog are obtained by using GPS after drilling. The drill holes and the prospecting lines marked on the map were designed before drilling).

4. Results

In Leapfrog software, the geographic locations of drill holes are defined by the Collar.csv file containing each hole's coordinate information. In addition, the georeferenced map also shows the locations of exploration lines and drill holes. Therefore, we could double-check the correction of the locations after we imported drillhole data and the map by using Leapfrog (Fig. 3).

4.1. Lithologies

The geologic map shows the studied area is covered by Neoproterozoic granites. However, the drill holes reveal that four different episodes of granites, the Neoproterozoic, the early Jurassic, the late Jurassic, and the Cretaceous, exist underground (Fig. 4, 5).

4.2. Fault networks on the surface

No structural models have been applied to the Shizidun tungsten deposit due in part to the fault system in the study area being simple. The Shizidun deposit is considered as the eastern extension of the supergiant Shimensi W-Cu-Mo deposit where seven steep NW-trending torsional faults (Fs_1, Fs_7, Fs_9, Fs_{11}, Fs_{20}, and Fs_{23}) and a hydrothermal cryptoexplosive breccia zone are identified by using the traditional method of field mapping. Information such as the geometries of the faults, whether or not a fault is an important storage structure of the deposit, and how a fault controls the granitic intrusions and ore veins are obtained (Zhang et al., 2022), illustrating that a cluster of NNE-, NE-, and NNW-striking faults exist in the region (Fan et al., 2021).

Although rarely and small-scale faults are discov-

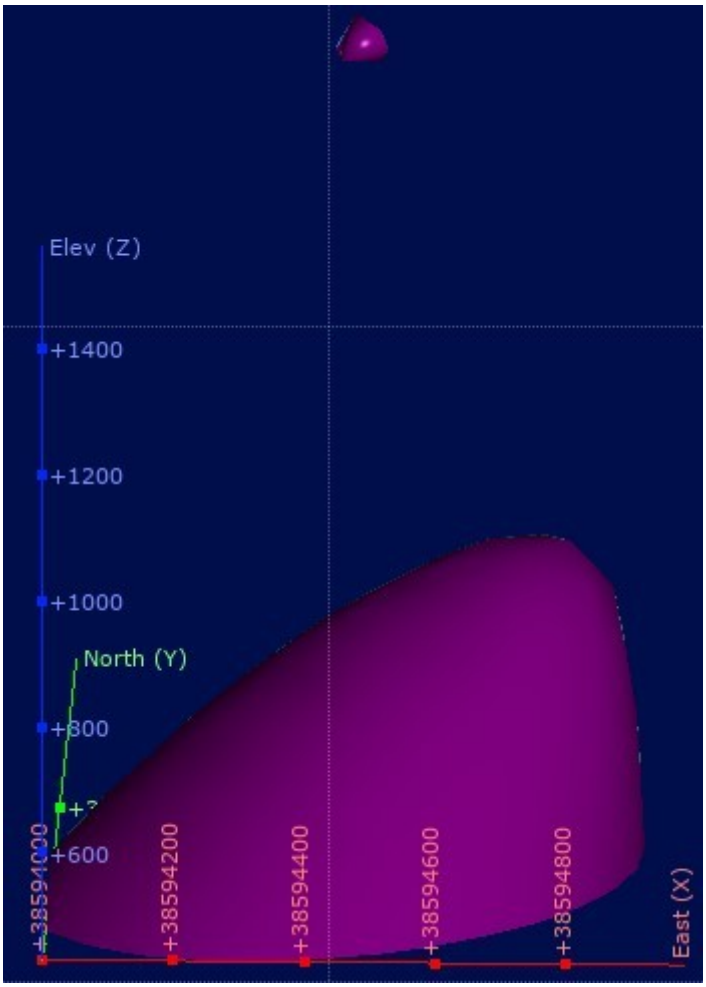

Fig. 4. Leapfrog reveals the volume and depth of the Cretaceous (top) and the Late Jurassic (bottom) granites by using drillhole data.

ered in Shizidun tungsten deposit, however, the faults control tungsten mineralization in the region. For instance, some faults are the storage structure of the Shimensi W-Cu-Mo deposit (Zhang et al., 2022). Furthermore, two sets of faults (a set of NEE-striking, and SSE-trending share zone were intersected by another set of NNE-trending fault) control the occurrences of the deposits and Mesozoic granites(Fan et al., 2021; Mao et al., 2013; Sun et al., 2018; Zhang et al., 2018), playing the role of channels for ore-forming fluids (Fan et al., 2021; Sun et al., 2018). In the giant Dahutang ore field, wolframite-scheelite quartz veins distribute primarily along the NNE- and NNW- striking faults. The stockwork fractures control the veinlet-disseminated mineralization (Xiang et al., 2012; Zhang et al., 2018). Last but not least, our analysis reveal that the average concentration of W from the fractured rocks is about 0.08 (%), almost ten times higher than the average abundance of W (0.0096%) of the Shizidun deposit.

The cropped-out faults were mapped from field measurement. We digitized the fault plane orientations by using ArcMap. The structural data including dip directions, dip angle, elevation, and coordinate information were input into Microsoft Excel to make a CSV file, producing the stereonet plot (Fig. 6) by using the software Stereo 32 (Institute of Geosciences, University of Sao Paulo, 2025)

The georeferenced map was imported along with the digitised fault plane orientations, and the structural data into Leapfrog. The fault locations and geometries are defined (Fig. 7).

The geological model almost does not change after addition of the fault information collected from the field measurement. Two reasons for this result could be: first, the Neoproterozoic granite almost covers the whole study area. Second, the small-scale surface faults, embedded within voluminous Neoproterozoic granite, lack sufficient displacement to alter the regional model, as confirmed by the digital elevation

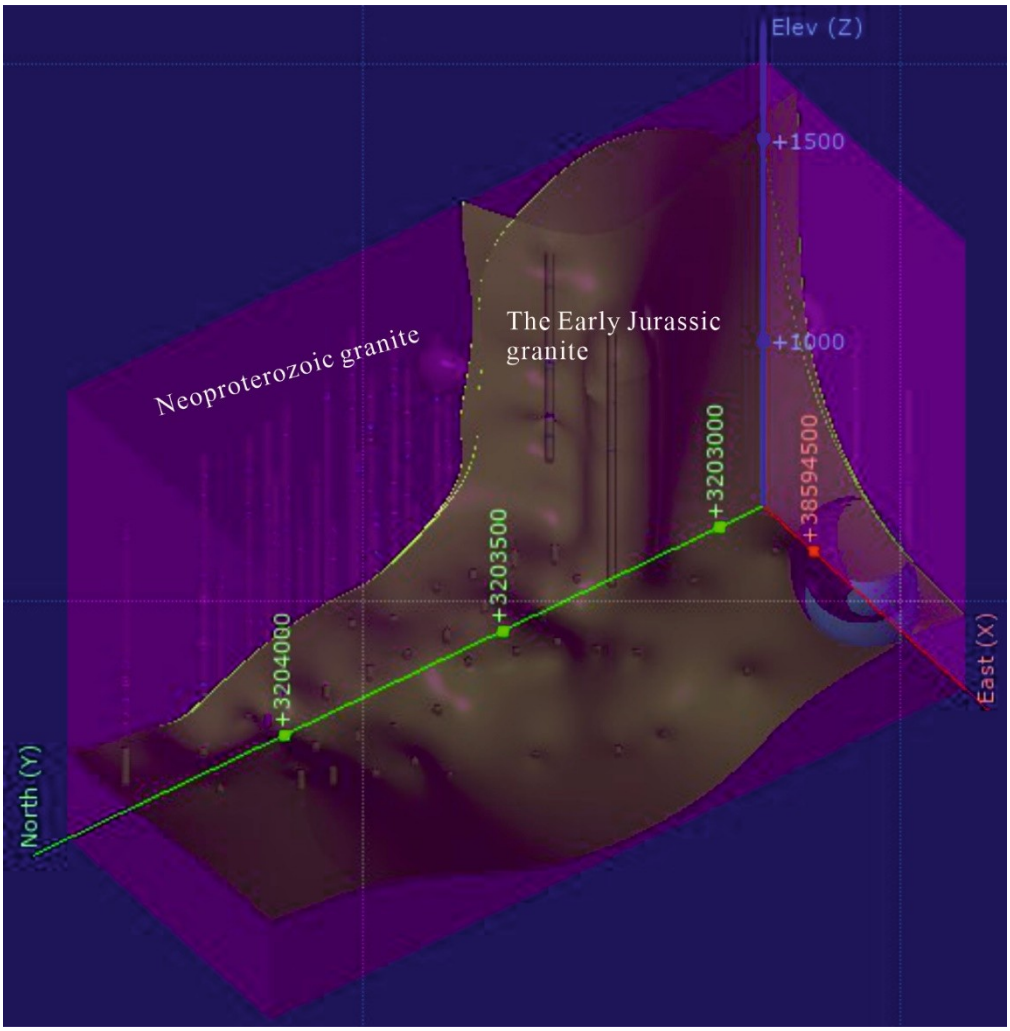

Fig. 5. 3D geologic modelling reveals that the explored area is dominated by Neoproterozoic granite but intruded intensively by the Early Jurassic granite.

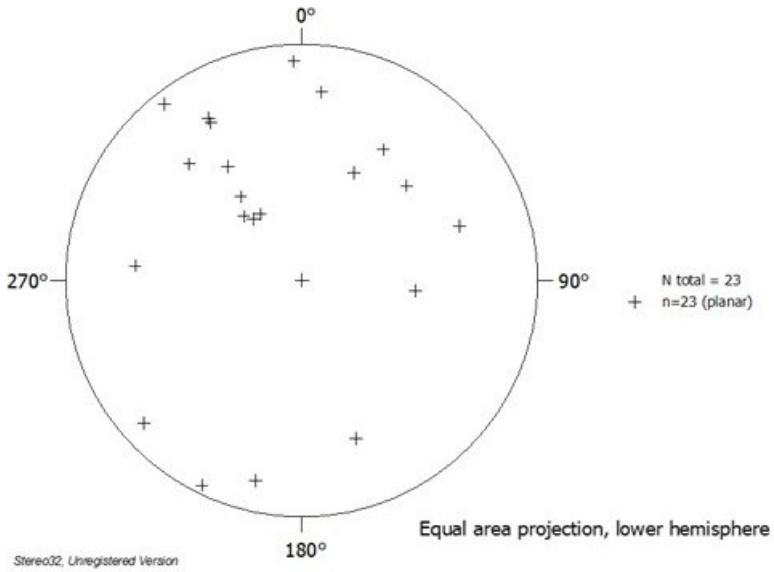

Fig. 6. Stereonet diagram of the faults observed in the surface of the Shizidun deposit. The data for stereonet projections were collected from the field trip.

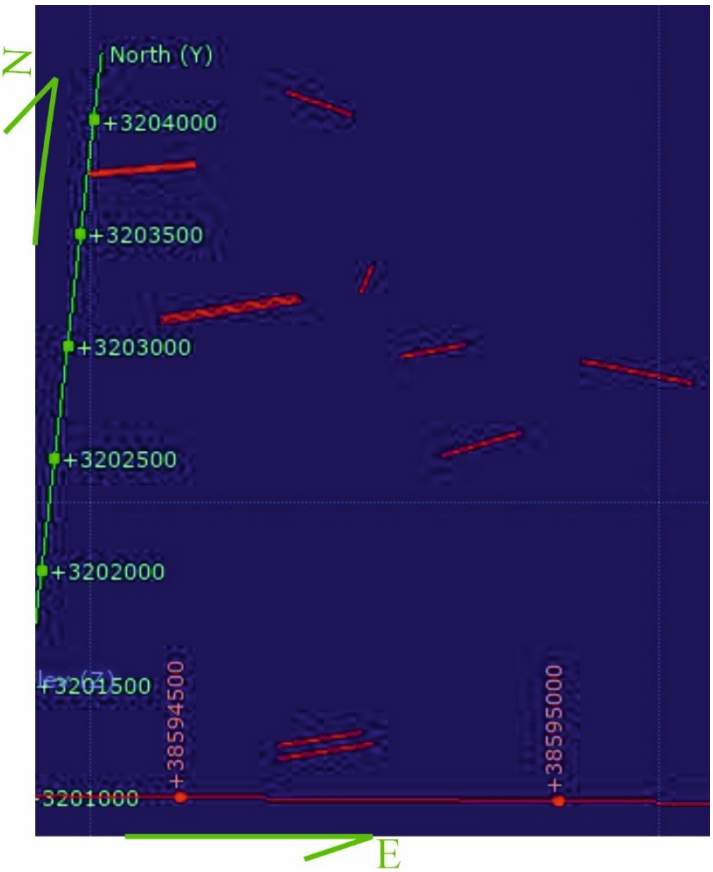

Fig. 7. Geographic locations of surface faults, connecting to a CSV file containing the data such as the dips and dip directions for leapfrog.

model (DEM) analysis (Fig. 8). Therefore, all the small-scale faults occur in the voluminous granite, resulting in no effect from surface faults in the geological model.

4.3. Fault networks underground

Although the small-scale surface faults had minimal impact on the geological model which is dominated by Neoproterozoic granites, drillhole logs reveal that the fractured rocks are indicative of subsurface faults. We modelled these underground fault networks using the fractured rock data. Given the scarcity of surface faults, identifying subsurface networks proved challenging, but we analyzed and categorized the fractured rocks into distinct fault sets prior to modelling. This process generated a 3D representation of the subsurface geological environment (Fig. 9).

The orange and magenta surfaces represent fault planes, which are discontinuities in the rock layers caused by tectonic movements. The faults appear to be steeply dipping and intersect in a complex pattern, indicating multiple faulting events or a highly deformed zone which are not revealed by surface geologic mapping (Fig. 9). The intersection of the orange and magenta surface suggests a network of faults with varying orientations and displacements. The complex fault pattern may correlate with the E-W strike-slip faults reported in adjacent areas (Fan et al., 2019, 2021), suggesting a shared tectonic history. The vertical alignment of some fault planes suggests they may be high-angle faults, consistent with the structural data from field measurement.

5. Conclusion

We modelled the lithology and fault networks using Leapfrog drillhole data, revealing the complexity of underground geological characteristics in the study area which cannot be observed from field investigation. We discovered that the study area is primarily covered by Neoproterozoic granite. However, a minor volume of Cretaceous and Late Jurassic granites exists underground. In addition, the Early Jurassic granites greatly intruded the Neoproterozoic granite.

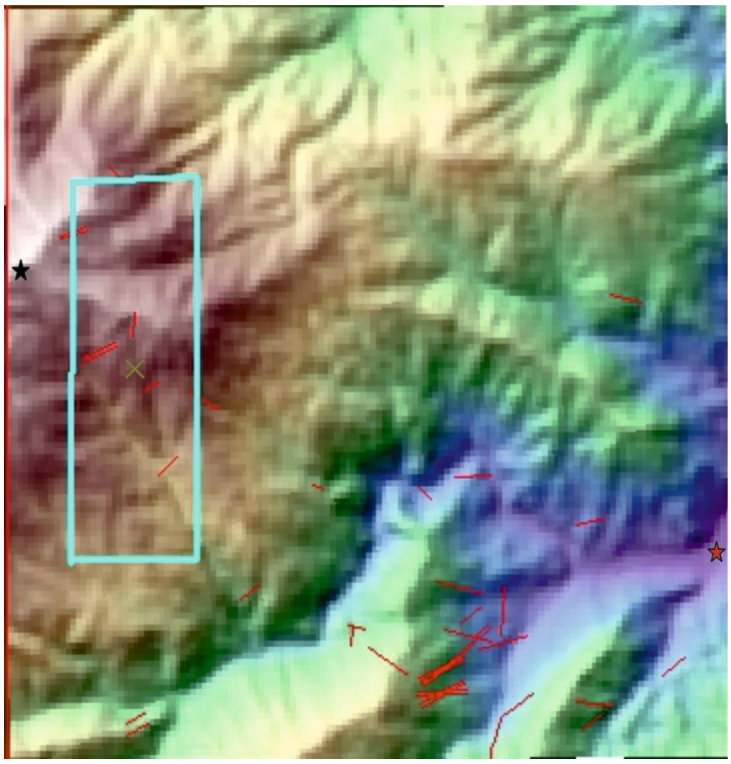

Fig. 8. The small-scale of surface faults shown on DEM, where the black star (brown coloured area), red star (blue coloured area), and the rectangle represent the highest land, the lowest land, and the area for the geological model in this study. The DEM is obtained from OpenTopography (Opentopography, 2025).

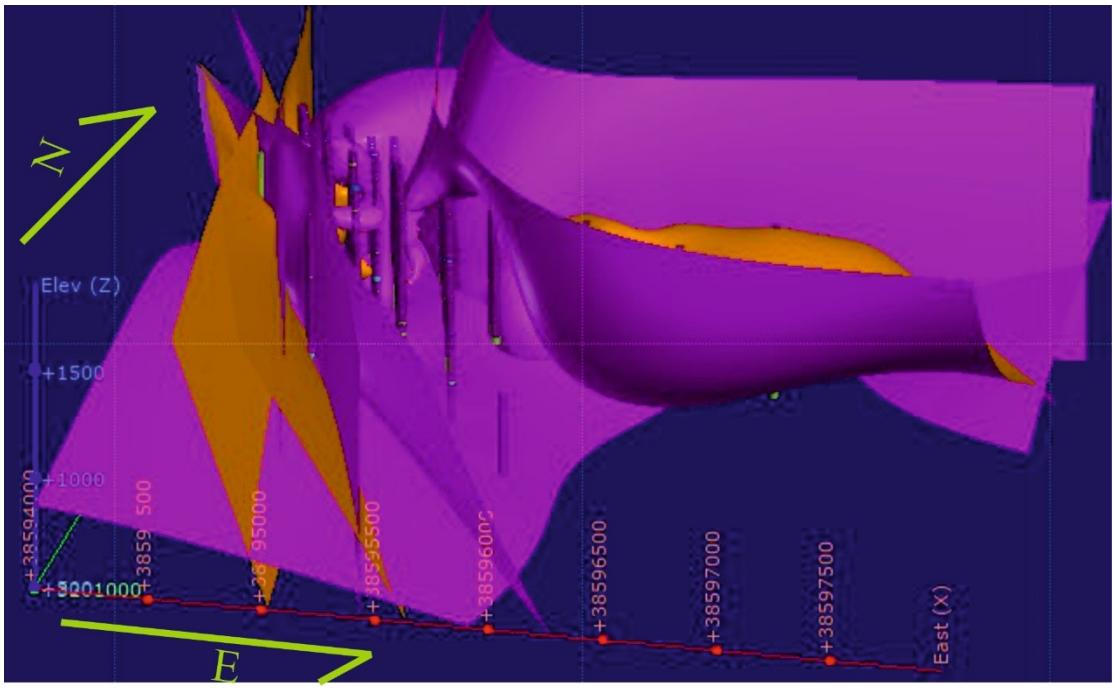

Fig. 9. Subsurface fault networks revealed by Leapfrog by using drillhole data (each polygon represents a set of fault).

Field investigation identified a handful of small-scale faults dipping at high angles with various strike directions on the surface. However, a lot of fractured rocks are discovered from drilling logs. Leapfrog models the subsurface fault networks, unveiling the subsurface geological complexity. These insights can guide targeted drilling and improve geohazard mitigation strategies. Future studies could incorporate

geophysical data to refine fault geometries and assess geohazard risks.

Acknowledgments

This work was supported by the National Key Research and Development Program of China (2023YFC2906803), the Scientific Program of Jiangxi Bureau of Geology (2024JXDZKJRC05), the Foundation of Jiangxi Educational Committee (GJJ2202914), the Start-up Funding for Research of Nanchang Institute of Science and Technology (NGRCZX-21-06), and the University's Project for Research of Nanchang Institute of Science and Technology (NGKJ-21-05).

CRediT statement

Mabi A W: Conceptualization, Methodology, Formal Analysis, Writing—original Draft, Software, Funding Acquisition. **Yu N B**: Project Administration, Funding Acquisition, Investigation, Formal Analysis, Validation, Editing. **Zhong H**: Project Administration, Investigation, Formal Analysis, Validation. **Chen D K**: Investigation, Formal Analysis, Validation. **Tong J Z**: Investigation, Formal Analysis, Ore reserve estimation, Validation. **Yu L B**: Investigation, Drilling Logs, Drawing, Validation.

Declaration of competing interest

The authors declare that they have no known competing financial interests or personal relationships that could have appeared to influence the work reported in this paper.

References

ESRI, (March 6, 2025). ArcGIS. Retrieved from https://www.esri.com/en-us/arcgis/geospatial-platform/overview.

Fan, X.K., Mavrogenes, J., Hou, Z.Q., Zhang, Z.Y., Wu, X.Y., Dai, J.L., 2019. Petrogenesis and metallogenic significance of multistage granites in shimensi tungsten polymetallic deposit, Dahutang giant ore field, South China. *Lithos* 336-337, 326–344. doi:10.1016/j.lithos.2019.04.001.

Fan, X.K., Zhang, Z.Y., Hou, Z.Q., Mavrogenes, J., Pan, X.F., Zhang, X., Dai, J.L., Wu, X.Y., 2021. Magmatic processes recorded in plagioclase and the geodynamic implications in the giant shimensi W–Cu–Mo deposit, Dahutang ore field, South China. *Journal of Asian Earth Sciences* 212, 104734. doi:10.1016/j.jseaes.2021.104734.

Institute of Geosciences, University of Sao Paulo, . (April 3, 2025). Open Stereo. Retrieved from https://igc.usp.br/openstereo/download/.

ARANZ Geo Limited, 2015. Tutorials for Leapfrog Geo version 3.0. ARANZ Geo Limited documentation, Christchurch, New Zealand. URL: https://help.seequent.com/Tutorials/Geo/3.1/en-GB/LeapfrogGeoTutorials.pdf.

Mao, Z.H., Cheng, Y.B., Liu, J., Yuan, S.D., Wu, S.H., Xiang, X.K., Luo, X.H., 2013. Geology and molybdenite Re–Os age of the Dahutang granite-related veinlets-disseminated tungsten ore field in the Jiangxin Province, China. *Ore Geology Reviews* 53, 422–433. doi:10.1016/j.oregeorev.2013.02.005.

Opentopography, (March 1, 2025). Find topography data. Retrieved from https://portal.opentopography.org/datasets.

Sun, K.k, Chen, B., Deng, J., Ma, X.h, 2018. Source of copper in the giant Shimensi W-Cu-Mo polymetallic deposit, South China: Constraints from chalcopyrite geochemistry and oxygen fugacity of ore-related granites. *Ore Geology Reviews* 101, 919–935. doi:10.1016/j.oregeorev.2018.08.029.

Wei, W.F., Shen, N.P., Yan, B., Lai, C.K., Yang, J.H., Gao, W., Liang, F., 2018. Petrogenesis of ore-forming granites with implications for w-mineralization in the super-large shimensi tungsten-dominated polymetallic deposit in northern Jiangxi Province, South China. *Ore Geology Reviews* 95, 1123–1139. doi:10.1016/j.oregeorev.2017.12.022.

Xiang, X.K., Liu, X.M., Zhang, G.N., 2012. Discovery of Shimensi super-large tungsten deposit and its prospecting significance in Dahutang area, Jiangxi Province. *East China Geology* 3, 141–151. doi:10.3969/j.issn.1671-4814.2012.03.002. (in Chinese with English Abstract).

Zhang, Q., Zhang, R.Q., Gao, J.F., Lu, J.J., Wu, J.W., 2018. In-situ LA-ICP-MS trace element analyses of scheelite and wolframite: Constraints on the genesis of veinlet-disseminated and vein-type tungsten deposits, South China. *Ore Geology Reviews* 99, 166–179. doi:10.1016/j.oregeorev.2018.06.004.

Zhang, Z.H., Zhang, D., Xiang, X.K., Zhu, X.Y., He, X.L., 2022. Geology and mineralization of the supergiant Shimensi granitic-type W-Cu-Mo deposit (1.168 Mt) in northern Jiangxi, South China: A review. *China Geology* 5, 510–527. doi:10.31035/cg2022036.

